Deposition and recirculation of tritium in the North Pacific Ocean

Sheila Stark[1]
Southampton Oceanography Centre, University of Southampton Waterfront Campus, Southampton, UK

William J. Jenkins and Scott C. Doney
Woods Hole Oceanographic Institution, Woods Hole, Massachusetts, USA

Received 30 September 2003; revised 17 February 2004; accepted 10 March 2004; published 4 June 2004.

[1] Tritium data, primarily from the GEOSECS and WOCE cruises of the 1970s and 1990s, are used to estimate the time-evolving ^{3}H inventory of the North Pacific basin. In the years between the two surveys, there have been changes both laterally and vertically in the distribution of ^{3}H in the North Pacific that reflect the mean circulation and exchanges of the basin. We develop a simple multibox model of the shallow circulation of the North Pacific to explore the long-term redistribution and changes in ^{3}H inventories within the basin. To do this, we derived a new estimate of the delivery of bomb ^{3}H to the North Pacific by precipitation for the period 1960–1997 and include other minor sources such as rivers. Vapor deposition dominates over direct precipitation of tritium to the basin, while inputs from continental runoff and the inflow from the south contribute over an order of magnitude less. The model predicted tritium budget of 25.1 ± 3.3 kg compares well with the estimated WOCE inventory of 23.4 ± 2.0 kg. We explore in detail the sensitivity of the budget calculations to model circulation and assumptions, as well as uncertainties in observations. We find that the ratio of tritium in vapor to that in precipitation is the most sensitive variable in the model budget, and the basin tritium inventory is consistent with a vapor-to-precipitation ratio of 0.67 (range 0.60–0.74), predictably somewhat less than the isotopic equilibrium value of 0.89. An inverse calculation shows that despite uncertainties in the tritium source function, the data also help constrain aspects of the basin circulation, including the Indonesian Throughflow. *INDEX TERMS:* 4808 Oceanography: Biological and Chemical: Chemical tracers; 4860 Oceanography: Biological and Chemical: Radioactivity and radioisotopes; 4532 Oceanography: Physical: General circulation; 4283 Oceanography: General: Water masses; *KEYWORDS:* transient tracer, ocean circulation, ventilation

Citation: Stark, S., W. J. Jenkins, and S. C. Doney (2004), Deposition and recirculation of tritium in the North Pacific Ocean, *J. Geophys. Res.*, *109*, C06009, doi:10.1029/2003JC002150.

1. Introduction

[2] Along with radiocarbon and CFCs, tritium (^{3}H) is the most well measured transient tracer in the modern ocean. The ^{3}H samples collected as part of the World Ocean Circulation Experiment (WOCE) provide us with the most extensive data set of this isotope presently available. In particular, the WOCE data set allows the North Pacific ^{3}H inventory to be calculated with much better accuracy than ever before (~10% as shown below) and to thereby constrain circulation issues for the basin associated with tropical-subtropical exchange, the Indonesian Throughflow, and intermediate water formation.

[3] Since large quantities of tritium were released into the atmosphere by thermonuclear weapons tests in the 1950s and 1960s, the isotope has proved to be a useful tracer of geophysical processes. Tritium is an ideal oceanographic tracer whose behavior away from the ocean surface is solely the result of radioactive decay, mixing, and the movement of water masses. The hemispheric asymmetry of the ^{3}H input function and the distinct Northern Hemisphere "spike" in 1963 due to atmospheric weapons testing clearly distinguishes the isotope from CFCs and makes it a valuable diagnostic of ocean general circulation models (OGCMs). Much of the "bomb" ^{3}H that has reached the oceans has already decayed, but it is, and will remain for several decades, a useful water mass tracer.

[4] Modeling efforts over the last 2 decades provide an increased understanding of the pathways by which tracers reach the ocean interior and the timescales of key oceanic processes. It has been argued that chemical tracers can constrain models in a way that temperature and salinity (T-S) alone cannot [*England and Maier-Reimer*, 2001]. However, at present the significant uncertainties associated with the surface boundary conditions for transient tracers greatly reduces their utility in formal inverse and data

[1]Now at Hadley Centre for Climate Prediction and Research, Exeter, UK.

0148-0227/04/2003JC002150$09.00

assimilation studies [e.g., *Memery and Wunsch*, 1990; *Li and Wunsch*, 2003]. For example, *Li and Wunsch* [2003] conclude that transient tracer fields provide little additional information on basin-scale circulation in the North Atlantic beyond that learned from hydrography alone. Instead, they use tracer observations primarily in the assimilation to adjust the more poorly known historical surface tracer fluxes. Improved analysis of tracer source function errors will provide, at a minimum, more realistic bounds for such data assimilation studies and will hopefully allow for the recovery of additional information of properties such as the water mass age distributions.

[5] Tritium entered the North Pacific via several pathways: precipitation, vapor deposition, lateral transport with the Arctic, South Pacific, and Indian Oceans, and river inflow. These four input pathways, along with advective transport, decay, and mixing within the North Pacific determine the temporal evolution of the ^{3}H concentration at any particular location in the basin. Ocean surface waters in the Northern Hemisphere had ^{3}H concentrations as high as 40 TU over the bomb spike in 1963–1964 compared to natural background levels of ~0.5 TU [*Michel and Suess*, 1975], where 1 TU = $^3H/^1H \times 10^{18}$.

[6] The distribution of tritium in North Pacific waters can be broadly understood by dividing the basin into three layers [*Fine et al.*, 1981]. The surface layer includes the depth range of the winter mixed layer within the subtropics and is therefore ventilated locally on an annual basis. This water has received ^{3}H directly from atmospheric fallout and lost some by lateral transport from the basin or exchange with deeper waters. Below this layer, the upper thermocline (second layer) receives ^{3}H from above and penetrates to the depth of the maximum winter outcrop isopycnal for the subpolar sector of the basin ($26.8\sigma_\theta$). Waters deeper than this isopycnal in the lower thermocline comprise the third layer and have only received ^{3}H by vertical diffusion or mixing, and intermediate water formation in the Sea of Okhotsk. In the 1990s, there was significant bomb ^{3}H at depth, indicating that the North Pacific can act as a sink for atmospheric constituents despite the lack of significant deep water formation in the area [*Fine et al.*, 1981].

[7] North Pacific tritium data have been used extensively to identify the pathways for water mass penetration into the subtropical gyre and the equatorial system [*Jean-Baptiste and Messias*, 1993]. Lateral advection along isopycnals transports ^{3}H from high latitudes to the subtropics and tropics [*Fine et al.*, 1981], and one of the most prominent features of the ^{3}H distribution in the tropics is the presence of a shallow subsurface tritium maximum centered between 125°W and 145°W. This has been interpreted as direct evidence of an "interior water pathway" from the subtropics to the equator [*McPhaden and Fine*, 1988; *Fine et al.*, 1987].

[8] *McPhaden and Fine* [1988] showed that the ^{3}H maximum is consistent with Sverdrup theory, which predicts a strong divergence of the North Equatorial Countercurrent (NECC) in the Central Pacific feeding an equatorial geostrophic mass flux. They postulated that it is this flow, which is dependent on the strength of the trade winds, that is responsible for the location of the ^{3}H maximum. Using a thermocline model and OGCM, *Liu and Huang* [1998] extended this work to incorporate the vertical structure of the geostrophic flow and to show that the ^{3}H maximum may be a result of transport both in the interior and along the western boundary, specifically in the Mindanao current. This process represents part of the North Pacific subtropical "Hadley" cell. Subduction of surface waters in the subtropics feeds a subsurface flow toward the equator where the water is upwelled. This water then moves poleward at the surface, subsequently affecting sea surface temperature and exchanging heat and freshwater with the atmosphere [*Johnson*, 2001]. The timescale for the subducted pathway has been inferred from ^{3}H measurements to be of the order 10 years [*Fine*, 1985; *Fine et al.*, 1987], and estimates of the magnitude of the flux are of the order 30 Sv (33.1 Sv [*Qiu and Huang*, 1995], 28.35 Sv [*Huang and Russell*, 1994]).

[9] The flow through the Indonesian Seas represents a path of surface and thermocline water transport from the Pacific to the Indian Ocean [*Fieux et al.*, 1996]. The magnitude of this transport is difficult to constrain, since the water passes through a complex series of channels with intricate topography and coastlines. This Indonesian Throughflow is driven by a pressure gradient between the western Pacific and the Indian Ocean set up by easterlies in the equatorial Pacific. North Pacific water is supplied to the throughflow by the Mindanao Current and Eddy [*Godfrey*, 1996; *Rodgers et al.*, 1999], which are part of the low-latitude western boundary circulation of the basin. Estimates of the magnitude of the throughflow vary widely, ranging from an estimate based on ^{3}H data of 5.1 Sv [*Fine*, 1985] through model-based estimates of a 9-year mean of 7.4 Sv [*Potemra et al.*, 1997] up to 16.4 Sv [*Morey et al.*, 1999]. The depth range of the flow is also much debated. It is often considered to be a warm surface water flow [*Morey et al.*, 1999], although some models suggest that more than half of the transport may occur below the mixed layer [*Fine*, 1985]. Also, there is significant seasonal and interannual variability in the magnitude of the throughflow associated with the regional monsoon and the El Niño Southern Oscillation [*Gordon*, 1986].

[10] One of the most striking features of the North Pacific subtropical gyre is a well-defined salinity minimum at depths of 300–800 m associated with North Pacific Intermediate Water (NPIW) [*Yasuda et al.*, 1996]. Intermediate water formation occurs in the North Pacific via ventilation in the subpolar gyre, especially in the Sea of Okhotsk, and is likely to be due to a combination of cooling and brine rejection during seasonal sea ice formation [*Reid*, 1965; *Warner et al.*, 1996]. Waters with a density greater than $26.8\sigma_\theta$ do not outcrop in the open North Pacific, but water densities up to $27.7\sigma_\theta$ are seen in the Sea of Okhotsk [*Talley*, 1991]. The general circulation in the Sea of Okhotsk is a broad cyclonic gyre [*Wong et al.*, 1998] connected to the North Pacific through the Kuril Islands. There are two direct ventilation sources in the basin at densities up to $27.05\sigma_\theta$, cold, fresh Dense Shelf Water formed on the northwest shelf by sea ice formation and warm, saline waters from the Japan Sea [*Itoh et al.*, 2003]. The outflow waters can sink to depths of 1000 m, though the effects can be spread to at least 2000 m by high rates of vertical mixing [*Talley*, 1991]. The presence of two ^{3}H maxima in the subpolar North Pacific suggests that North Pacific Intermediate Water (NPIW) that is formed in the northwest may be further ventilated downstream in the Gulf of Alaska [*Van Scoy et al.*, 1991]. It has also been proposed [*Talley*, 1993; *Talley and Yun*, 2001] that although direct ventilation is rare in the North Pacific outside of the

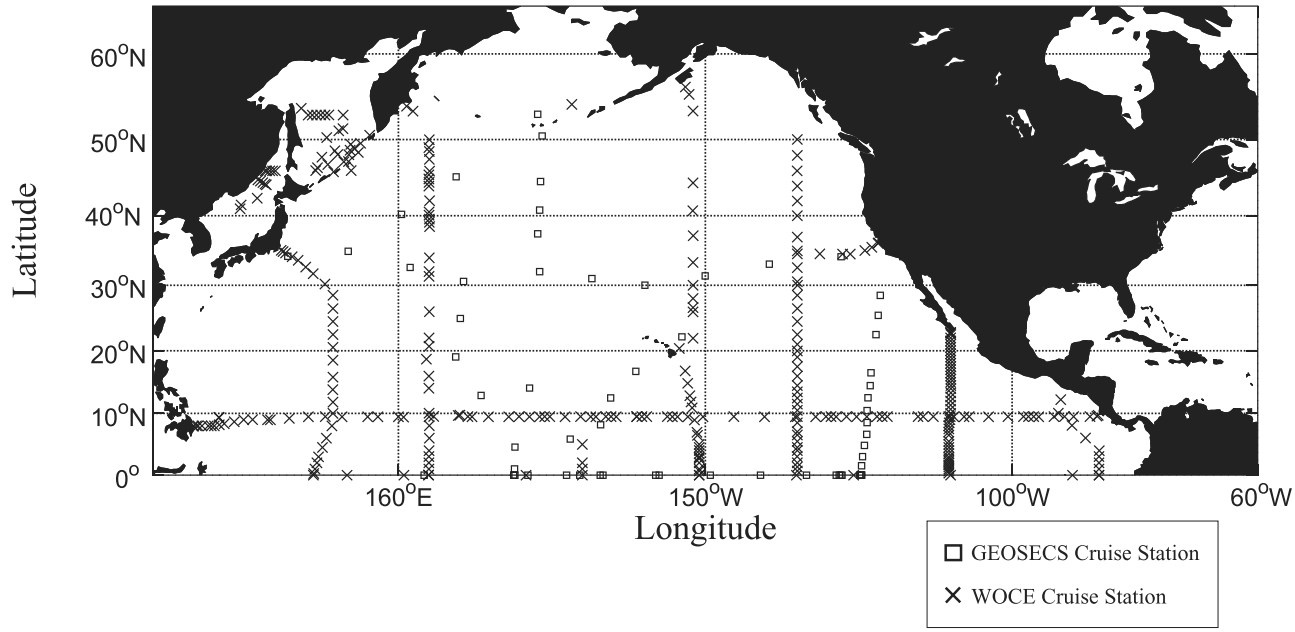

Figure 1. Map of the North Pacific basin showing the location of the sample stations on the WOCE and GEOSECS cruises. Much less data are available to calculate the GEOSECS inventory as there were only 42 stations in the North Pacific compared with 326 during the WOCE series of cruises. The boxes represent the bins that were used to calculate the overall inventory.

Sea of Okhotsk, intermediate water is also formed at fronts in the mixed water region (MWR), between the Oyashio and Kuroshio. In this area a salinity minimum is formed by the juxtaposition of relatively fresh subpolar surface waters beneath warmer saltier subtropical waters. *Talley* [1993] proposed that although the water initially lies at the density of the local subpolar winter mixed layer, it is quickly eroded from above, resulting in a salinity minimum at higher densities (NPIW). Both cabelling and double diffusion have been shown to contribute to this increase in density [*Talley and Yun*, 2001].

[11] In this study we explore the utility of tritium in circulation problems by developing an idealized model North Pacific ^{3}H budget that we compare to inventories calculated from the WOCE and GEOSECS cruise data sets. The usefulness of ^{3}H to such calculations is limited by how well one can constrain its input function. Therefore we derive a new estimate of the delivery of bomb ^{3}H to the North Pacific by precipitation, vapor deposition, rivers, and lateral advection for the period 1960–1997. Building on the work of *Doney et al.* [1992], we calculate a global model function of the ^{3}H distribution in precipitation using World Meteorological Organization (WMO)/International Atomic Energy Agency (IAEA) data. This model function allows the atmospheric delivery of ^{3}H to the North Pacific to be calculated using the standard *Weiss and Roether* [1980] hydrological model. We explore the sensitivity of the model to circulation and surface input assumptions with a view to ascertaining the usefulness of ^{3}H to such quantitative circulation problems.

2. North Pacific Tritium Inventories

[12] Two data sets were used to describe the changing North Pacific tritium inventory, namely the 1973–1974 GEOSECS (Geochemical Ocean Sections) and the 1989 to 1995 WOCE cruise data sets.

[13] Samples for the WOCE tritium data used here were collected between January 1989 and April 1995 and subsequently analyzed in the Woods Hole Oceanographic Institution Helium Isotope Laboratory. Samples were collected from 57°N to 50°S and in the Northern Hemisphere sampling extended longitudinally from 71.5°W to 126.5°E, making it the most detailed study of ^{3}H in this ocean so far. Samples were collected from throughout the water column down to a depth of 6089 m, although samples from depths greater than 3 km were taken sporadically for the purpose of estimating sampling and analysis blanks.

[14] The GEOSECS data was collected between January 1973 and October 1974, and sampling extended from the equator to 53.1°N. The longitudinal extent of these cruises was less than in the later WOCE survey, with few samples being taken from the western or the low-latitude eastern portions of the basin. The location of the sampling stations from both series of cruises is shown in Figure 1.

[15] For each data set the tritium inventory was calculated by vertically integrating the data at each station from the surface to the deep ocean and averaging over horizontal spatial bins that cover the basin, as shown in Figure 1. The data were decay corrected to a uniform date (1 January 1997: TU97) using the revised tritium half-life of 12.32 years [*Lucas and Unterweger*, 2000]. The decision to have fewer bins longitudinally was due to the poorer spatial resolution of the cruise stations in that direction. Uncertainties in the inventories were calculated from the standard deviations of the column-integrated values in each bin. Bins that contained no data were assigned a ^{3}H concentration by interpolating from surrounding bins, and the error was conservatively set as equal to this value. It is conceivable that the quoted errors are likely to be an

Table 1. Comparison of Observed North Pacific Tritium Inventories[a]

Data Set	Inventory, kg	Author
WOCE	23.4 ± 2.0	this study
GEOSECS	21.1 ± 4.7	this study
GEOSECS	16.2[b]	*Van Scoy et al.* [1991]
GEOSECS	16.3 ± 2.4[b] to 15°N[c]	*Broecker et al.* [1986]
	19.8 ± 3.0[b] to 10°S[c]	
Long Lines	15.8[b] ± 1.6[d]	*Van Scoy et al.* [1991]

[a]All values are corrected to 1 January 1997.
[b]These inventory calculations were not calculated using the revised tritium half-life of *Lucas and Unterweger* [2000]. Errors introduced by this will be less than 1%.
[c]Error value based on the quoted error for the global ocean of ~15%.
[d]Error value based on the quoted tritium sample measurement error of 10% (1σ). This is a minimum value as errors will also be introduced by the spline interpolation and spatial averaging procedures used to calculate the overall inventory.

underestimation of the total uncertainty, since no account was taken of the potential longitudinal variability of the ^{3}H distribution within the large 50° wide bins. Moreover, the approach may also lead to spatial biases, particularly in the GEOSCECS results where the sampling is very sparse.

[16] Table 1 shows the calculated, decay-corrected tritium inventories from the two data sets and compares them with those from earlier studies. All estimates of the North Pacific inventory calculated from data sets that pre-date the WOCE survey are smaller than the WOCE value. This is primarily a reflection of the improved sampling of the WOCE cruises. For example the northwest subpolar and subtropical gyres, regions that contain high water column ^{3}H inventories, are undersampled by the GEOSECS cruises, which could lead to low biases in calculated GEOSECS inventories.

[17] Strong spatial gradients exist in the distribution of ^{3}H in the North Pacific. Latitudinal variability which reflects the location of the thermonuclear weapons tests and the location of maximum ^{3}H rainout at midlatitudes is still very evident in the WOCE distribution, even after 3 decades of circulation and mixing. Earlier work has highlighted the importance of good longitudinal sampling as deeper ^{3}H penetration is seen in the west of the subtropical gyre following the downward slope of isopycnals from east to west [*Fine et al.*, 1981]. Much of the finer structure of the North Pacific ^{3}H distribution will have been missed by the GEOSECS cruises, as there were very few stations north of 40°N, with extremely sparse sampling in the west and northeast of the basin (see Figure 1). The WOCE data have also highlighted the importance of better depth sampling than in earlier studies as there is clearly ^{3}H at intermediate depths in the basin that needs to be included. The calculated value from the GEOSECS data is larger but broadly consistent with the values from *Broecker et al.* [1986] and *Van Scoy et al.* [1991] considering the large error in the calculated value. Unfortunately, direct comparisons are hard to make because the error fields are poorly defined for the earlier estimates.

[18] In summary, the greater uncertainty in the GEOSECS compared to the WOCE inventories is the result of the poorer spatial resolution and coverage of the GEOSECS cruises. This arises from the greater degree of interpolation and extrapolation required with the geographically sparser data set to estimate the basin scale inventories.

3. The Changing Distribution of Tritium in the North Pacific

[19] Within the uncertainties of the two inventory estimates (the larger error contribution being from the GEOSECS data), the tritium inventory has remained constant. This is in contrast to the North Atlantic, where a significant increase in the ^{3}H inventory over time is seen due to Arctic inflow [*Doney et al.*, 1993]. However, in the years between the two Pacific surveys, there have been significant changes both laterally and vertically in the water column distribution of ^{3}H in the North Pacific, which reflect the mean circulation of the basin.

[20] Comparing the latitudinal distribution of the decay-corrected tritium inventory in the North Pacific between GEOSECS and WOCE (Figure 2) shows that the bulk of the ^{3}H remains in the subtropical gyre (20°N–40°N), in good agreement with earlier studies [*Broecker et al.*, 1986; *Van Scoy et al.*, 1991]. Stronger latitudinal gradients are evident in the top 1000 m of the water column in the earlier GEOSECS data, which show a more pronounced subtropical maximum, reflecting the depositional pattern of bomb tritium. The loss of strong latitudinal gradients in the WOCE data is due to negligible ^{3}H entering the ocean in the intervening years coupled with continued homogenization by circulation and mixing. This reduction was already evident by the time of the Long Lines cruises in 1983–1985 [*Van Scoy et al.*, 1991]. The meridional variations seen in the WOCE data are more striking deeper in the water column, especially the pronounced maximum at 40°N–50°N below 1000 m (Figure 2) in comparison to the GEOSECS values which are quite low at that depth. This is clear evidence of an increase in depth penetration between the two surveys as is seen with bomb radiocarbon [*Peng et al.*, 1998].

[21] Overall, the depth distribution of decay-corrected tritium has not changed dramatically between the two surveys with the majority of the inventory being concentrated in surface waters, although there is deeper penetration in the WOCE data (see Figure 3). The highest concentrations are seen in surface waters, and there is little ^{3}H below 1000 m. In the WOCE data, there is more ^{3}H at intermediate depths with 23% of the inventory being at depths greater than 500 m compared with 11% in the GEOSECS data. The inventory depth profile at 0°–10°N shows that very little ^{3}H has penetrated below 1000 m and that it is truly a shallow water tracer in the tropics. In contrast the profiles at 30°N–40°N and 50°N–60°N show that at higher latitudes a greater proportion of the inventory is at intermediate depths, with detectable amounts of ^{3}H down to 2500 m. Although there is a more noticeable increase in depth penetration at high latitudes, there is a larger ^{3}H inventory between 500 m and 1000 m for 30°N–40°N than at 50°N–60°N. This pattern reflects the location of intermediate water formation in the subpolar gyre, especially in the Sea of Okhotsk and the Bering Sea [*Warner and Roden*, 1995], and its subsequent

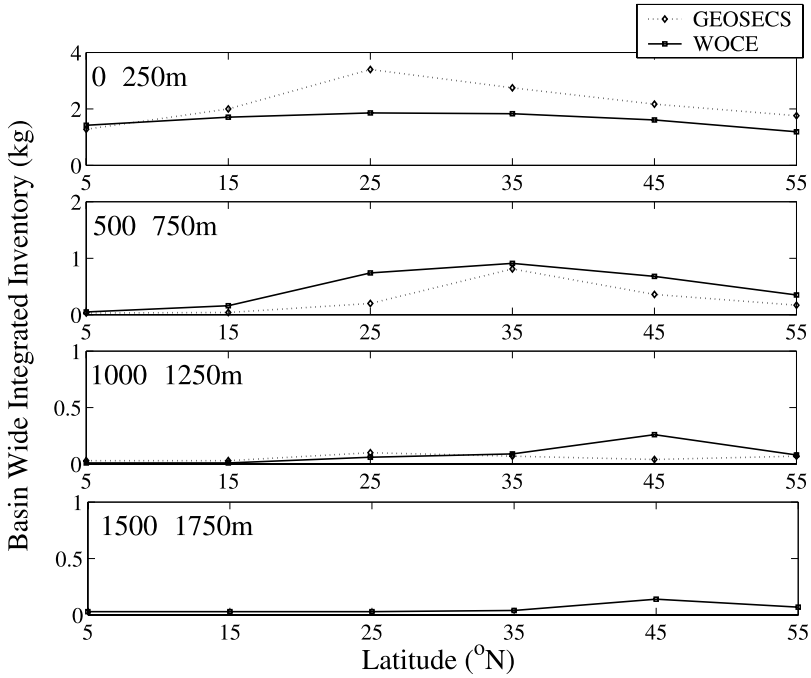

Figure 2. A WOCE and GEOSECS comparison of the latitudinal distribution of ^{3}H in the North Pacific at three different depths. Note the different inventory scale on each plot.

transport to and modification within the subtropical gyre [*Talley*, 1991].

[22] Figure 3 illustrates that by the time of the later survey, there is an increase in the amount of tritium in surface equatorial waters and a decrease in the shallow waters of the subtropical gyre. This shift of ^{3}H from middle to low latitudes is the result of a Hadley cell movement of properties from the subtropics to the tropics, a shift that is also seen in bomb radiocarbon [*Key*, 2001; *Mahadevan*, 2001].

[23] The improved estimates for the inventory and distribution of tritium in the North Pacific provided by the WOCE cruise data allow us to use the isotope to constrain circulation and total atmospheric deposition in the basin. To this end we developed a simple multibox model of the North Pacific to construct a ^{3}H budget to compare with the inventory results

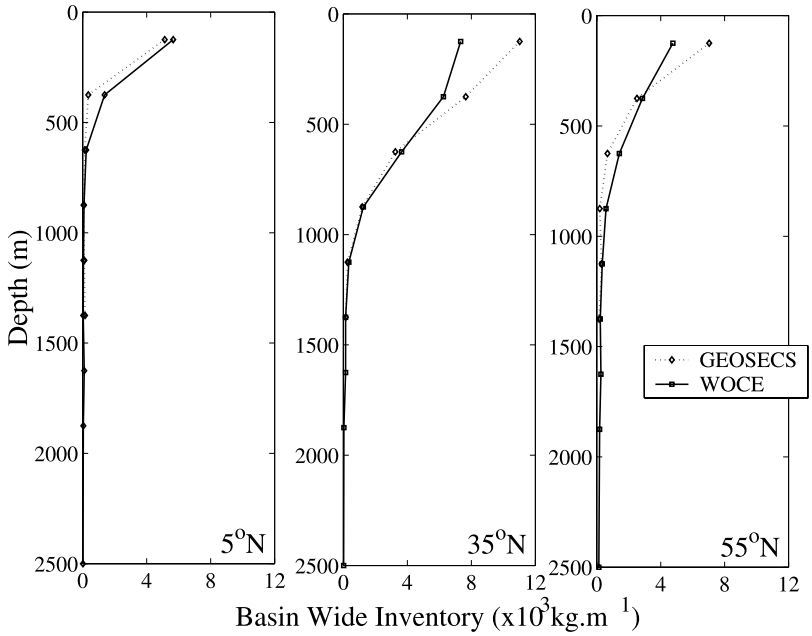

Figure 3. A WOCE and GEOSECS comparison of the depth distribution of ^{3}H in the North Pacific at three different latitudes.

(section 5). Prior to this, however, we present an improved model of tritium delivery by precipitation to the basin.

4. Atmospheric Tritium Deposition to the North Pacific

4.1. Total Atmospheric Deposition

[24] The total atmospheric delivery of tritium to the ocean consists of three components, the precipitation flux, the downward vapor flux, and finally the vapor back-flux from the ocean due to re-evaporation, such that

$$D_{atm} = PC_P + E\frac{h}{1-h}C_V - E\frac{1}{\alpha(1-h)}C_S, \qquad (1)$$

where E, P, and h are the hydrological parameters evaporation, precipitation, and relative humidity, C_P, C_V, and C_S are the tritium concentrations in precipitation, vapor, and surface water, respectively, and α is the isotopic equilibrium factor for HTO/H_2O in liquid-vapor exchange.

[25] This relationship was proposed by *Weiss and Roether* [1980] and *Weiss et al.* [1979], and it has become the generally accepted model for the tritium flux to the oceans. However, over recent years, several areas of the analysis, namely the C_V/C_P ratio, have been questioned [*Koster et al.*, 1989; *Memery and Wunsch*, 1990; *Doney et al.*, 1992]. *Weiss et al.* [1979] assumed that ^3H concentrations in marine precipitation and vapor are in isotopic equilibrium. This proposition was based on a limited number of simultaneous observations of vapor at ship's height and precipitation. The data show considerable scatter [*Roether*, 1989]. This assumption allows the ^3H concentration in vapor at any time t, $C_V(t)$, to be related to that in precipitation and set equal to $^1/_\alpha C_P(t)$ or $\sim 0.89\ C_P(t)$. It is important to consider the validity of this assumption over the bomb spike when precipitation ^3H concentrations were high. Such an assumption will have a significant effect on estimates of the total ^3H deposition. Considering equation (1), it is clear that as surface water ^3H concentrations are much smaller than those in precipitation, the third term represents a minor correction only. It also follows that as $E \approx P$ and $h \approx 0.75$ the input from vapor exchange should greatly exceed that from precipitation, so the chosen value of the C_V/C_P ratio is critical to the total calculated ^3H deposition.

[26] The work by *Jouzel et al.* [1987] showed that rain is never in complete isotopic equilibrium with water vapor, even at the sea surface, and that ^3H concentrations in rain are generally higher than in the surrounding water vapor. This can be expected because the atmospheric boundary layer water vapor inventory will be strongly affected by an evaporative flux of lower-tritium water from the sea surface. Unfortunately, there is very little data to quantify the degree of isotopic equilibration, and the lack of data means that a precise constraint on the vapor deposition to the world ocean is problematic. *Doney et al.* [1993] compared the water vapor ^3H data of *Östlund and Mason* [1985] from Baring Head Lighthouse New Zealand with monthly precipitation data from the nearby ($\sim$50 km) Kaitoke weather station. This resulted in a mean C_V/C_P ratio of 0.81 ± 0.03, which was taken to be more representative of pure maritime conditions than Miami ($C_V/C_P = 0.60 \pm 0.05$), a location that experiences both maritime and continental air masses.

Table 2. Summary of the Work Done to Date on the Relationship Between the Tritium Concentration in Water Vapor (C_V) and Precipitation (C_P)

Source	C_V/C_P Ratio
Isotopic equilibrium	0.89
Koster et al. [1989] (model)	0.35 ± 0.05
Weiss et al. [1979] (data)	0.76 ± 0.05
Doney et al. [1993] using *Östlund and Mason* [1985] Miami data	0.60 ± 0.05
Doney et al. [1993] comparison of *Östlund and Mason* [1985] data with IAEA precipitation at Baring Head Lighthouse New Zealand	0.81 ± 0.03

Table 2 summarizes the values of the C_V/C_P ratio from models and data that are presently available.

[27] There is a substantial difference between values of the C_V/C_P ratio calculated from observations and the atmospheric modeling result of *Koster et al.* [1989]. The smaller simulated value may be due to the model having insufficient water vapor transport into the atmospheric boundary layer, as it appears that the model's downward vapor transport is too slow. Also, the model had a limited representation of continental re-evaporation and did not recreate the large gradient between continental and marine precipitation [*Roether*, 1989]. The vertical flux of ^3H in the atmosphere is affected by the phase of the condensate as the isotope is much freer to exchange and escape to the surrounding atmosphere from raindrops than falling ice particles. Modeling studies need a careful treatment of the isotopic adjustment of ^3H between rain/ice and vapor since this process allows ^3H to escape from the condensate and ultimately reach the surface in vapor form.

[28] In their tritium budget for the North Atlantic, *Doney et al.* [1993] used a C_V/C_P ratio of 0.7 ± 0.1, the mean of the values from Miami, New Zealand, and the *Weiss et al.* [1979] results. The same value is used here to calculate the atmospheric delivery of ^3H to the North Pacific.

[29] It is also important to note that the C_V/C_P ratio is unlikely to be constant and likely has changed over the course of the tritium transient [*Doney et al.*, 1993]. As surface water ^3H concentrations increase relative to those in precipitation, the ratio is likely to increase as the vapor back flux from the ocean surface becomes increasingly tritiated.

4.2. Precipitation

[30] The concentration of tritium in precipitation that is needed to compute the atmospheric deposition of ^3H to the North Pacific was calculated using a global ^3H precipitation model function. Following the work of *Doney et al.* [1992], the global distribution of ^3H in precipitation can be modeled using R-mode factor analysis.

[31] To produce the model function, the WMO/IAEA tritium in precipitation data set from 1960 to 1997 was used. Data before 1960 were excluded as insufficient data were collected before this year. The IAEA data set is sparse in both space and time, and measuring stations are unequally spaced around the globe (Figure 4) and do not cover the same time periods at all stations. Moreover, there are few stations away from the continental margins. In this study, only the 93 stations with at least 5 years of ^3H data including the major bomb transient between 1962 and 1964 were used. The aim of the model function was to

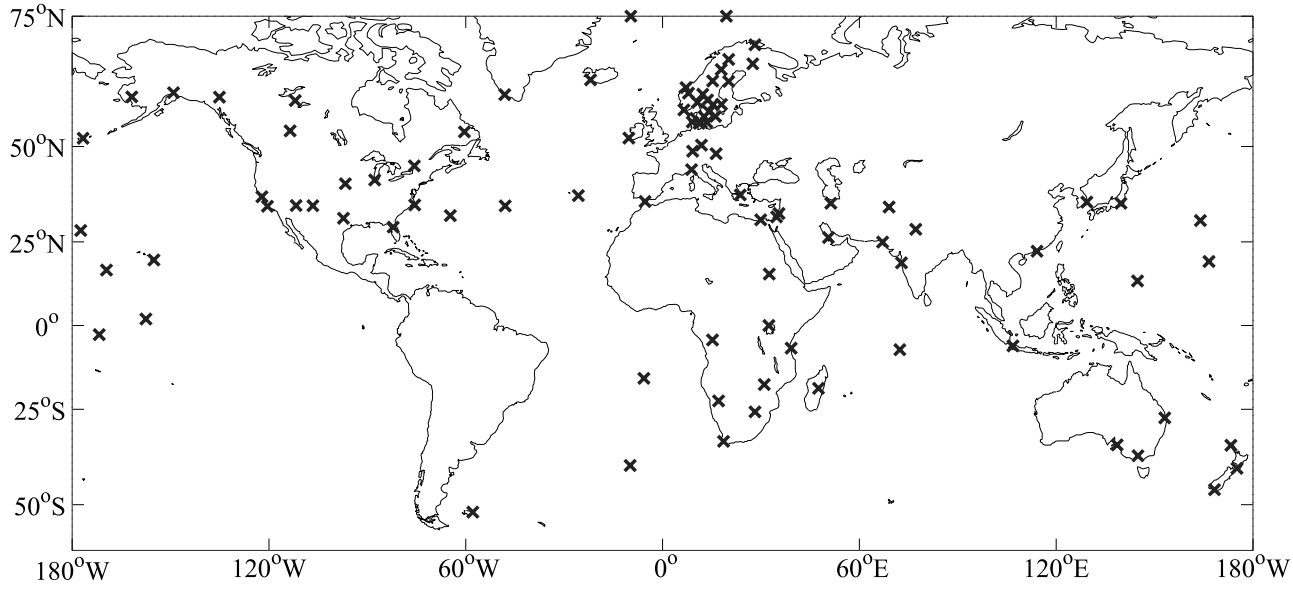

Figure 4. A map showing the location of the WMO/IAEA sampling stations used to construct the ^{3}H in precipitation model function. It is clearly visible that the majority of the stations are located on the continents in the Northern Hemisphere. Of the 93 sampling stations included in the model, only 16 are at ocean island locations that can be termed truly oceanic.

construct a set of reference curves that could be used to estimate the ^{3}H time history in precipitation at any location.

[32] To account for the sparse coverage of the station data, the annually averaged tritium concentrations were zonally averaged into 10° latitude bands from 50°S to 70°N. A simple linear interpolation was used to account for areas with very sparse data. These steps resulted in zonal mean ^{3}H concentrations which could be represented by $C_P(t, \varphi)$, a 38 × 12 matrix. Building on the work of *Doney et al.* [1992], this was modeled in *R*-mode factor analysis as a linear combination of n factors such that

$$C_P(t,\varphi) = \sum_{i}^{n} \left(\hat{c}_p(t,i) l(i,\varphi)\right) + \varepsilon(t,\varphi). \quad (2)$$

In equation (2), $\hat{c}_p(t, i)$ is the ith vector of the factor scores (the time records from 1960 to 1997), $l(i, \varphi)$ is the ith vector of the factor loadings (the latitudinal patterns from 50°S to 70°N), and $\varepsilon(t, \varphi)$ is the error matrix.

[33] Before doing the factor analysis, the data were normalized to have a variance of one and a mean of zero. This was done by subtracting the mean over all years from each latitude band and then dividing by the standard deviation. If this step were ignored, the weaker, more diffuse Southern Hemisphere signal would be overwhelmed by the larger Northern Hemisphere spike.

[34] The covariance matrix of $C_P(t, \varphi)$ was then solved for its eigenvectors, and the n eigenvectors with the largest eigenvalues were retained as the n factors of $C_P(t, \varphi)$. The n eigenvectors were then varimax rotated to localize the variance from each latitude band onto a smaller number of factors. As can be seen from Figure 5, three factors account for more than 96% of the original variance in $C_P(t, \varphi)$. Their resulting factor loadings ($l(\varphi)$) and factor scores ($\hat{c}_p(t)$) are shown in Figure 6.

4.2.1. Factor Distributions

[35] The characteristics of the factors can be explained in terms of the global hydrological cycle of tritium. As can be seen from Figure 6, the temporal and spatial distributions of the first two factors are broadly consistent with the *Doney et al.* [1992] analysis and can be interpreted as a Northern Hemisphere (factor 1) and a Southern Hemisphere (factor 2) factor. The time history of the first factor shows the expected Northern Hemisphere spike in 1963, while the second factor shows the delayed and more diffuse signal that is typical of the Southern Hemisphere, arising because of the slow communication between the stratospheres of the two hemispheres and the onset of weapons testing south of the equator in 1968 [*Taylor*, 1971]. The dominance of the Northern Hemisphere factor, which accounts for 76% of the variance in $C_P(t, \varphi)$, is a reflection of the location of the largest bomb tests in the Northern Hemisphere, the penetration of this signal well into the tropics, and weighting of the zonal average data set toward the Northern Hemisphere.

[36] The third factor, which was not seen in the *Doney et al.* [1992] analysis, shows a peak that precedes the main pulse of the first factor in 1963. This may be a reflection of near-field tropospheric fallout occurring soon after the first bomb tests. For example, debris from the Bravo Test of 1954 was rapidly removed by ice crystals formed by the large quantities of seawater carried aloft by the bomb cloud [*Taylor*, 1966]. The deposition of ^{3}H to the Earth's surface is composed both of this early fallout and the delayed stratospheric component. Evidence of the importance of direct, early deposition is seen in the WMO/IAEA data from Taguac, Guam. As is shown in Figure 7, the ^{3}H in precipitation records from this island in the North Pacific show high ^{3}H concentrations in 1961 and 1962 prior to the main, Northern Hemisphere peak signal in 1963.

4.2.2. Discussion of Model Function Performance

[37] Using equation (3), the annual mean tritium concentration at an individual station $c_P(t)$ can be calculated from a

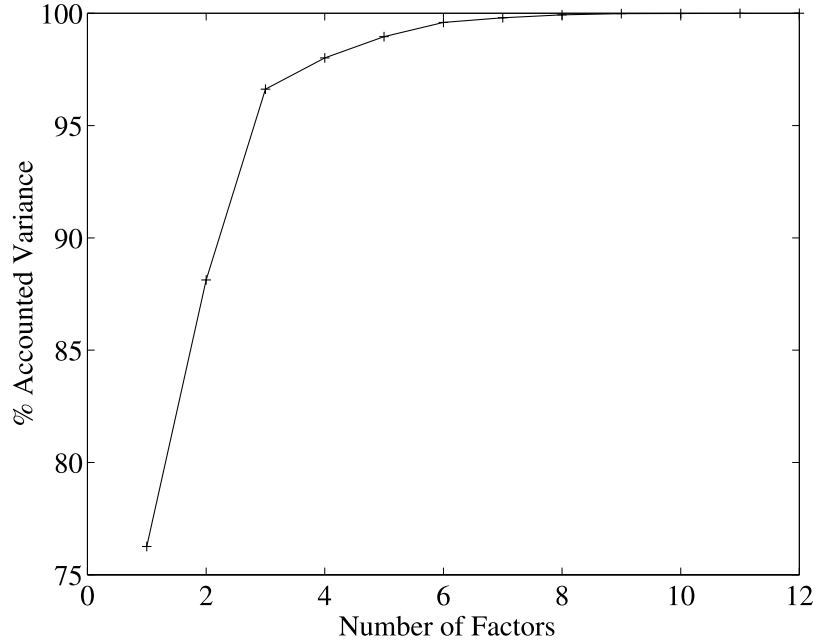

Figure 5. Plot of the variance accounted for versus the number of factors for the factor analysis of zonally averaged tritium data.

linear combination of the three reference curves $\hat{c}_P(t, 1)$, $\hat{c}_P(t, 2)$ and $\hat{c}_P(t, 3)$ such that

$$c_P(t) = f_0 + f_1\hat{c}_P(t,1) + f_2\hat{c}_P(t,2) + f_3\hat{c}_P(t,3) + \varepsilon_a(t). \quad (3)$$

The three coefficients (f_1, f_2 and f_3) and mean (f_0) are unique for each individual station and were calculated from the least squares solution of equation (3). The residual error, $\varepsilon_a(t)$, represents the mismatch between the reconstruction and the measured data at each station. For each station, the standard deviation of the residuals was estimated as a measure of the goodness of the fit from equation (3) such that

$$\sigma_a = \left(\frac{1}{N-4}\sum_{i=1}^{N}\varepsilon_a^2\right)^{\frac{1}{2}}, \quad (4)$$

where N is the number of years (in the variable t_i) for which there is ^{3}H data at a particular station.

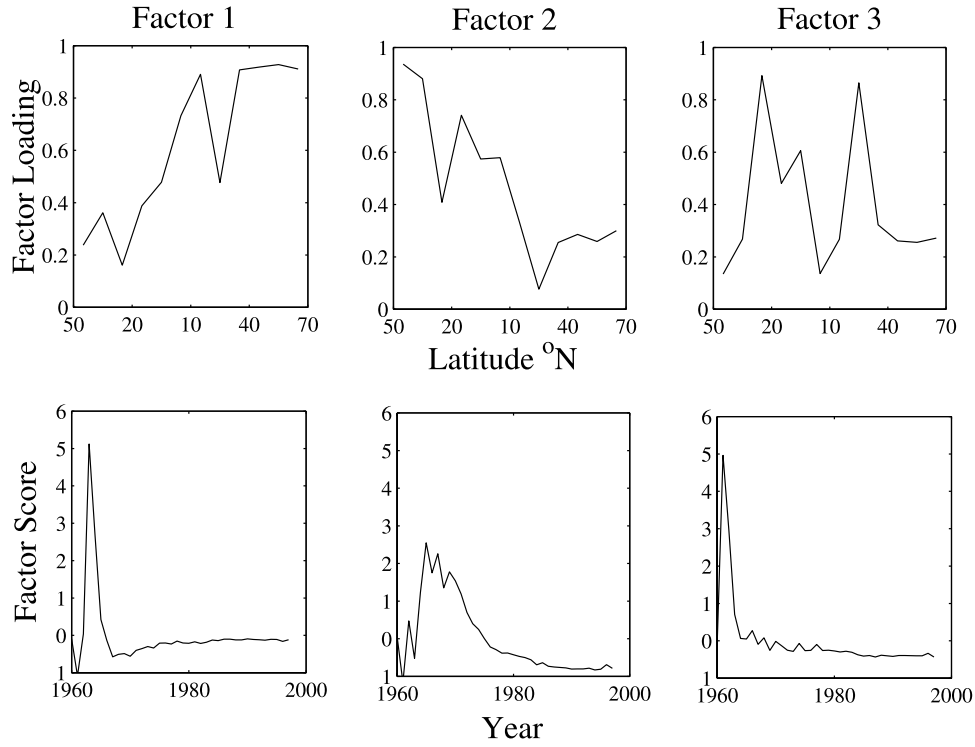

Figure 6. Factor loadings and factor scores calculated for the zonally averaged tritium data.

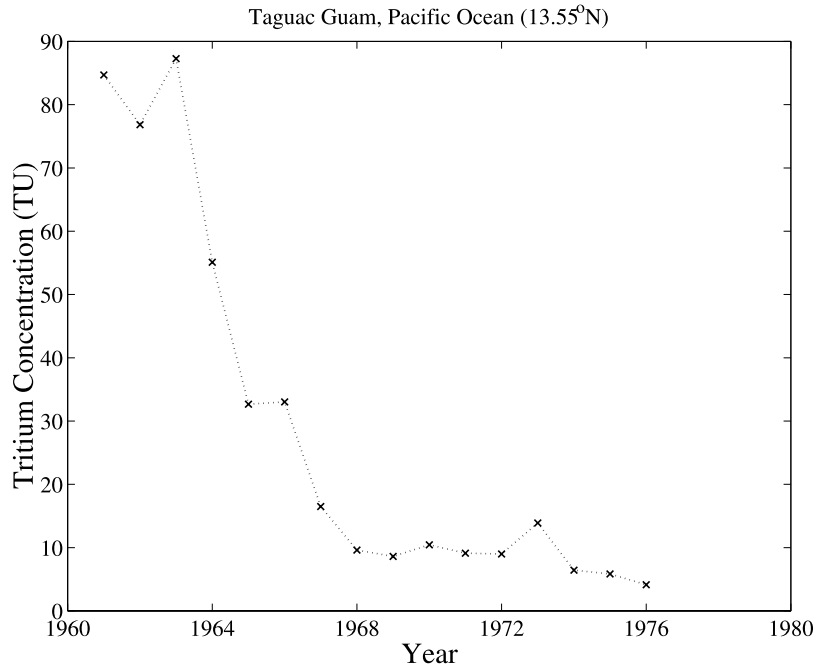

Figure 7. Tritium in precipitation concentrations recorded at Taguac Guam Island in the North Pacific Ocean. The peak in tritium concentrations is clearly visible preceding the main bomb spike in 1963. Data were only collected at this location between 1961 and 1976.

[38] The performance of the model at two key stations, both of which have long duration precipitation records are shown in Figure 8. It is clear that the model recreates well the annual ^{3}H in precipitation time histories at both a Northern Hemisphere location (Valentia) and a Southern Hemisphere location (Kaitoke), each of which has a small standard deviation (9.62 TU and 2.42 TU, respectively) compared to their respective signal sizes. Good model

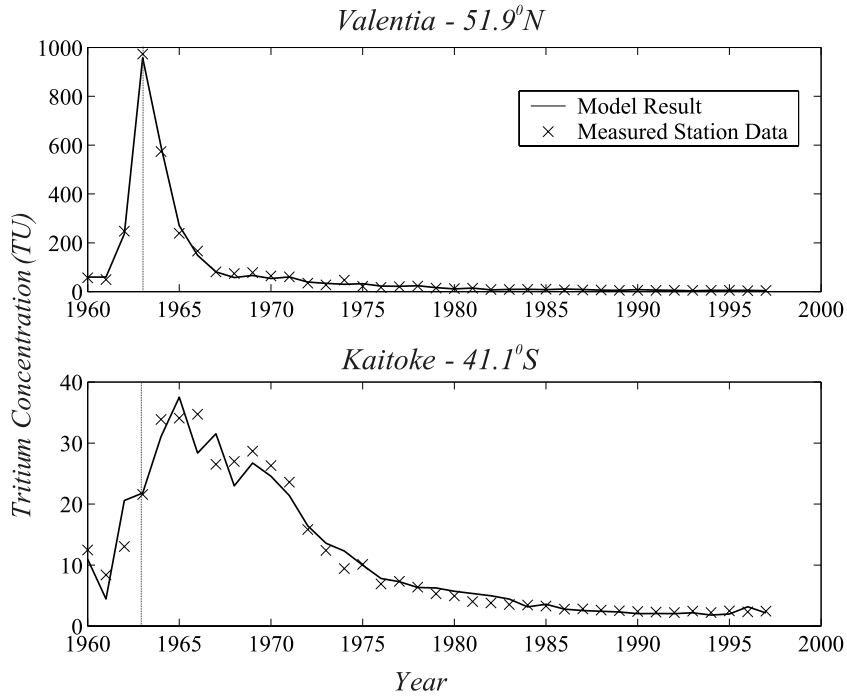

Figure 8. Model function performance compared with data at two continental locations, Valentia (Ireland) and Kaitoke (New Zealand). The Northern Hemisphere bomb spike in 1963 is clearly marked in both plots by a dotted line. Note the very different concentration scales on the two plots, which is a reflection of the much higher tritium in precipitation concentrations in the Northern Hemisphere.

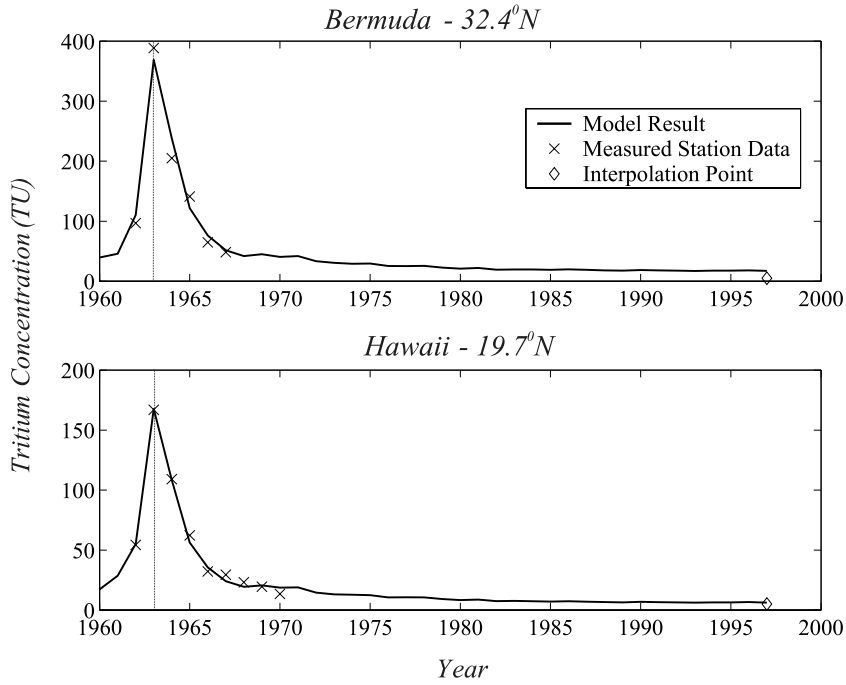

Figure 9. Model function performance compared with data at two oceanic locations, Bermuda (North Atlantic) and Hawaii (North Pacific). Again, the two plots have different concentration scales reflecting the strong latitudinal gradient of the tritium concentration in precipitation. The bomb spike in 1963 is marked by a dotted line. Included in the plot is the interpolation point that was used to improve model performance at locations where data are sparse.

performance is typical of continental sample stations, where there is plenty of raw data, though neither Valentia or Kaitoke can be considered truly continental as they both have coastal locations. To prevent the model overestimating the ^{3}H concentration at stations with temporally sparse data after the spike, such as Bermuda and Hawaii (see Figure 9), a simple linear interpolation was fitted to a typical pre-bomb concentration of 5 TU in 1997. As is shown by Figure 9, this allows the model to perform well at these two typical oceanic locales.

[39] The tritium time-history at any arbitrary point on the globe can be estimated by spatially interpolating the three coefficients f_1, f_2, and f_3 for the ^{3}H reference curves derived for the individual stations and then calculating a new time-history using equation (3). When calculating the deposition to an individual basin, such as the North Pacific, a number of issues arise which reflect the sparse global sampling network, strong latitudinal gradients, and the marked transitions between oceans and land in the ^{3}H precipitation record. Of the 93 stations included in the model, only 16 are truly oceanic (island), and several are in coastal locations, which are likely to move in and out of the continent-marine boundary layer. This is a major weakness of this model function as ^{3}H concentrations in precipitation are typically 2–5 times higher over the continents than the oceans at the same latitude [*Doney et al.*, 1992]. This contrast is the result of the faster removal of HTO and larger water vapor levels over the oceans compared with the continents.

[40] The length scale for the continental/marine transition was estimated to be of order 1000 km [*Weiss and Roether*, 1980], but the spatially interpolated model exhibits a much broader layer due to the lack of available data from stations at oceanic locations. This effect can be corrected for by adjusting the computed $c_P(t)$ fields to take into account how far the continental ^{3}H signal penetrates over the oceans. In lieu of suitable ^{3}H data, this penetration distance can be estimated from precipitable water (w) data [*Doney et al.*, 1993]. Precipitable water represents the amount of liquid water that would result if all of the water vapor in the atmosphere were condensed [*Peixoto and Oort*, 1983]. Evaporation over the oceans, especially in the subtropics, increases the precipitable water (net E-P) and lowers the water vapor ^{3}H concentration through dilution and ocean uptake. Hence the length-scale over which the continental ^{3}H signal is removed should be comparable to or less than that of the transformation of low w continental air into high w marine air [*Doney et al.*, 1993]. The transition in w extends 500–1000 km from the continents [*Prabhakara et al.*, 1982], and a length scale of 500 ± 250 km was used in the model calculations as in the *Doney et al.* [1993] North Atlantic ^{3}H budget. Using this length scale, the precipitation input to the North Pacific was calculated by assuming that the ^{3}H profile falls off exponentially from the precipitation function continental end-member to a minimum marine value, taken from the available WMO/IAEA oceanic station data.

[41] The total atmospheric deposition of tritium to the North Pacific was calculated using equation (1) with $C_V/C_P = 0.7 \pm 0.1$. The hydrological parameters were taken from the *Da Silva et al.* [1994] climatology, and the

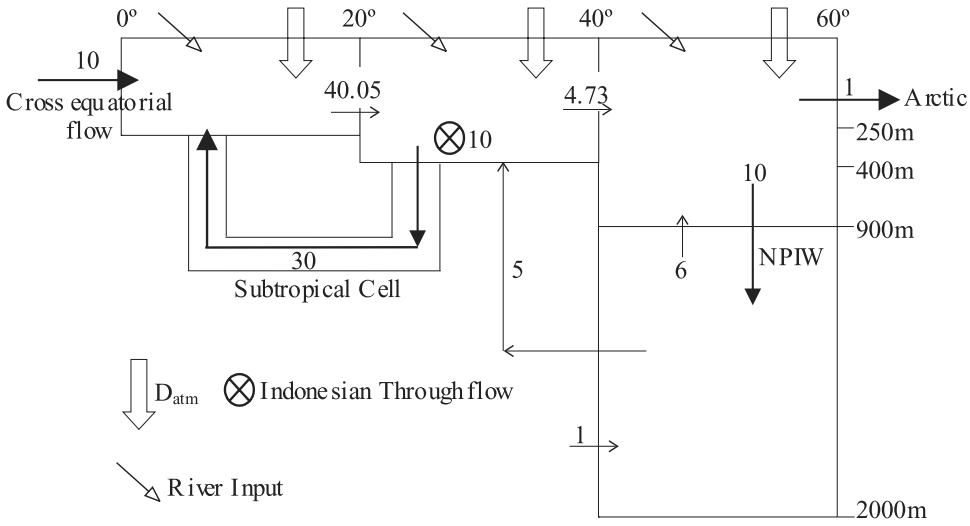

Figure 10. Schematic of the multibox model of the shallow circulation of the North Pacific. All of the fluxes are in Sv (1 Sv = 1 × 10^6 m^3 s^{-1}), and the model was run with a time step of 0.5 years. The timescale of subtropical-tropical exchange is of order 10 years [*Liu and Philander*, 2001] and the model subtropical cell applies a 10-year delay to waters flowing from the subtropics to the tropics. After formation, NPIW is transported to and modified within the subtropical gyre, where it is seen as a low-salinity signal [*Talley*, 1991].

deposition was calculated over a 2.4° grid for the North Pacific from the equator to 60°N.

5. Model of the North Pacific Tritium Budget

[42] A simple multibox model of the circulation of the North Pacific was developed to use the calculated WOCE inventory and regional patterns to constrain the atmospheric and advective terms in the tritium budget. Once developed, some of the flows in this general kinematic model were modified to match the available ^{3}H data.

5.1. Continental Runoff of Tritium to the North Pacific

[43] The input of tritium to the North Pacific from continental runoff is very small compared with that from the atmosphere, so a simple runoff scheme was deemed sufficient. The flux was calculated using the *Weiss and Roether* [1975] river model and the land precipitation ^{3}H concentrations C_P. The calculated ^{3}H concentration time histories for the major rivers that drain into the North Pacific were multiplied by *Baumgartner and Reichel* [1975] annual runoff volumes to get annual ^{3}H runoff fluxes into each of the model boxes. The model is very simple and may only be applicable to midlatitude rivers such as the Rhine; tropical and high-latitude rivers will behave in a qualitatively different manner [*Doney et al.*, 1993]. For example, high-latitude rivers such as the Amur may have shorter residence times and lower groundwater contributions because of subsurface permafrost layers [*Östlund*, 1982].

5.2. Kinematic Model

[44] To calculate the total atmospheric deposition of tritium to the North Pacific, a box model of the shallow circulation was used to simulate the surface water time histories needed to calculate the re-evaporation term. The basin was split into tropical, subtropical, and subpolar boxes, the depth of which were chosen on the basis of observed ^{3}H distributions and on what is known about the circulation and hydrography. The tropical box was chosen to extend to 20°N to include the North Equatorial Current (NEC), which is the northernmost current of the equatorial system flowing westward between 10°N and 20°N. The subtropical box extends to 40°N, beyond which constitutes the subarctic region [*Michel and Suess*, 1975], separated from the subtropical gyre by an abrupt change in temperature and salinity.

[45] The model circulation, including all advective fluxes, is shown in Figure 10. It was constructed to conserve water. An inflow of water from the South Pacific is needed to balance the flow of North Pacific water into the Indian Ocean [*McCreary and Lu*, 2001]. To calculate the ^{3}H flux into the model from its southern boundary, the water flux (10 Sv) was multiplied by a time history of ^{3}H concentrations in the equatorial South Pacific. This time history was constructed from data from the top 250 m of the water column from the WOCE, GEOSECS, and RSMAS series of cruises. The northward surface flows in Figure 10 have been adjusted to account for the net input of mass to the basin from rivers and the balance of precipitation and evaporation.

5.3. Model Tritium Budget

[46] The results of the North Pacific Budget Model are shown in Figures 11 and 12. Figure 11 shows the annual ^{3}H contribution from each of the terms in the model. It is clear that the main source of bomb ^{3}H to the North Pacific has been atmospheric vapor deposition, which exceeds direct precipitation by a factor of 2. This is consistent with earlier work [*Doney et al.*, 1993], which found that ^{3}H by vapor deposition exceeds that by direct deposition by a factor of 2–5. A ratio at the lower end of this range may be expected in the North Pacific because of its large ocean to coastline ratio, which allows evaporation from the sea surface to have a significant effect on the oceanic, near-surface water vapor

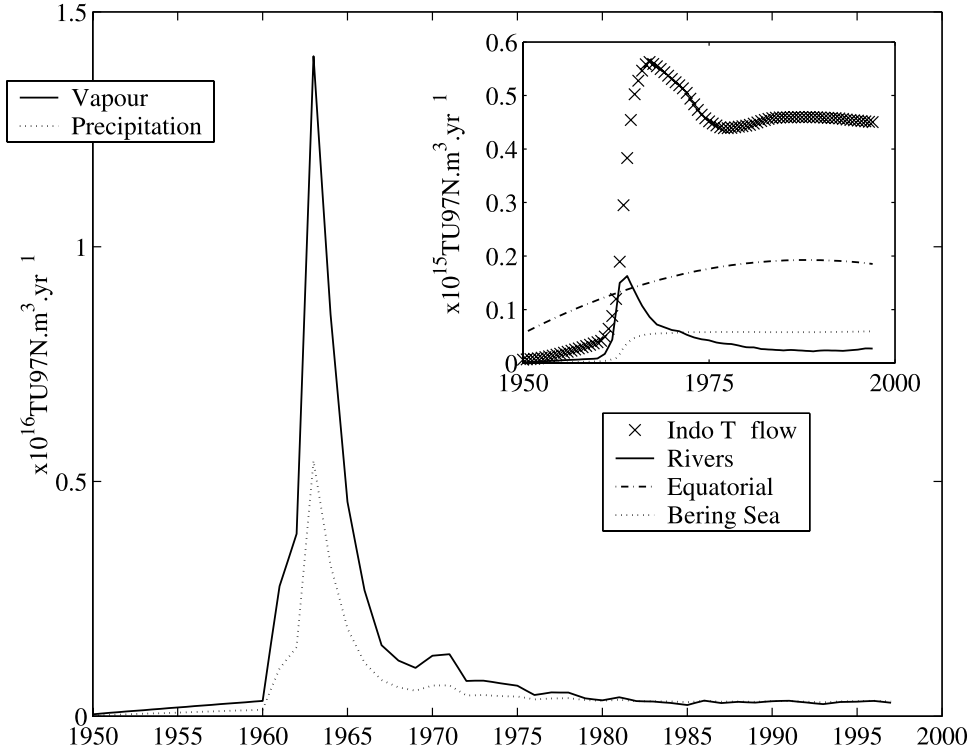

Figure 11. Time histories of the atmospheric deposition and advective terms in the model North Pacific budget.

concentration. After 1980, deposition from direct precipitation starts to exceed the net vapor input, which reflects the growing relative importance of the vapor back flux term after the main bomb spike.

[47] Inputs from rivers and the modeled circulation contribute over an order of magnitude less than the atmospheric deposition to the overall budget, with the loss through the Indonesian Throughflow contributing more than the other

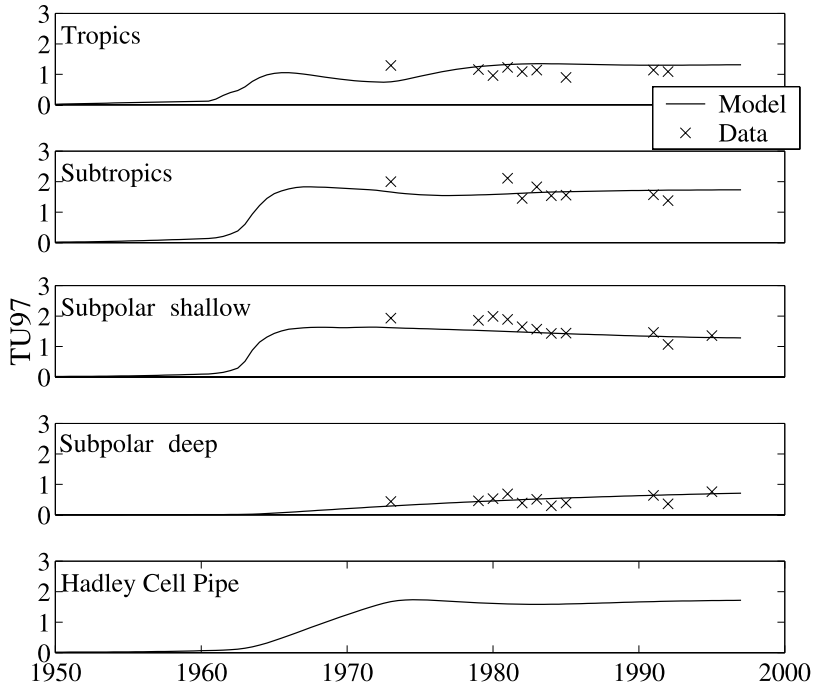

Figure 12. Model tritium concentrations time histories for the four boxes in the model and the lower limb of the Hadley cell. For each box, the concentration shown is the average over the bounding boxes shown in Figure 10. Data come from the WOCE, GEOSECS, and RSMAS (Rosenstiel School of Marine and Atmospheric Sciences, University of Miami) cruises.

Table 3. A Comparison of the Original and Inverse Model Inventories With Those Calculated From the WOCE Cruise Data[a]

Area	WOCE Inventory, kg	Original Model, kg	Inverse Model, kg
Tropics	5.36	6.60	5.87
Subtropics	10.09	9.54	9.17
Subpolar shallow	6.09	6.55	5.65
Subpolar deep	1.90	2.46	2.43
Subpolar total	7.99	9.01	8.08
North Pacific	23.40	25.10	23.12

[a]The inverse model is described and discussed in section 6.

advective terms. The maximum river contribution is seen to lag the atmospheric spike, since 35% of the water in the river model has a residence time of 5 years and consequently shows a delayed and broader ^{3}H peak than precipitation and vapor deposition. The importance of the river contribution to the budget is minimal after the delayed main bomb spike. The relative importance of the advective terms to the budget increases after 1975 as deposition continues to decline after the main bomb transient. In particular, the Indonesian Throughflow and cross-equatorial ^{3}H input become comparable in importance to atmospheric deposition after this year.

[48] The model output can also be used to evaluate the changing distribution of ^{3}H in the North Pacific. Figure 12 and Table 3 show that the majority of the bomb ^{3}H remains in the upper ocean with the highest concentrations being seen in subtropical waters, reflecting the location of the bomb tests and of maximum stratospheric-tropospheric exchange. The maximum in the surface box ^{3}H concentrations is seen to lag the atmospheric spike of 1963 by 2 to 3 years, consistent with the work of *Fine and Östlund* [1977]. The increase in the amount of ^{3}H at intermediate depths in the subpolar region is a reflection of intermediate water formation. There is a net movement of ^{3}H from the subtropics to the tropics, which is in agreement with the WOCE observations. The model produces a double peak in the tropical box time history due to the delayed arrival of the tritium input via the subtropical cell. A delayed but weaker signal is also seen in the subtropical box due to the surface limb return flow of the Hadley cell.

[49] The overall tritium inventory for the North Pacific calculated from the model is 25.1 ± 3.3 kg which falls within the error margins of the WOCE inventory value of 23.4 ± 2.0 kg. The error in the model inventory is derived by combining the uncertainties in each of the advective and atmospheric deposition terms in the model assuming they are uncorrelated.

[50] This good agreement, within errors, between the model and WOCE inventories indicates that generally the model is working well, with a realistic amount of ^{3}H present in the North Pacific basin. It is also clear from the good broad agreement between the model and cruise concentrations in Figure 12 and inventories in Table 3 that the model produces a reasonably realistic distribution of ^{3}H in the basin. From the mid-1980s onward, the original model somewhat overestimates the concentrations and WOCE inventories in the tropical and shallow subpolar boxes by 10–20%. Examination of Table 3 reveals that the inventory in the deep subpolar box is also overestimated by the model. These local discrepancies between the model and WOCE data indicate that there are some problems with the way ^{3}H is redistributed within the model basin. The error may reflect regional variability in the atmospheric deposition. Both the value of the C_V/C_P ratio and the continent-marine transition length scale may not be the same for each of the model boxes. For example, in the subpolar box, where the model overestimates the inventory, there is only one oceanic station in the WMO/IAEA precipitation data set north of 40°N which is located at the edge of the marine boundary layer and therefore may not be truly representative of open ocean conditions.

[51] Alternatively, the ^{3}H distribution may be reflecting errors in the model's circulation and transport. The overestimation of the tropical inventory coupled with the underestimation of that in the subtropical box could be evidence of an overly vigorous Hadley cell or weak Indonesian Throughflow in the model. Likewise, the overestimation in the deep subpolar box could reflect an unrealistic representation of the formation and modification of NPIW. The sensitivity of the model to each of these terms is further explored using inverse techniques.

6. Inverse Calculation

[52] The sensitivity of the model to each of the major advective and atmospheric terms was explored using an inverse calculation. The prime objective of the inverse was to improve the model's total and regional distribution of ^{3}H. The system is overdetermined and poorly conditioned, and therefore the parameters were determined in a least squares fashion. The constraints for the inverse were the WOCE regional inventory values, as this captures all of the information available for the WOCE period, namely the total inventory and regional distribution.

[53] The control variables for the calculation were the atmospheric deposition (namely the C_V/C_P ratio) and the advective fluxes (Table 4). The cost function reads

$$J = (I_{R_{\mathrm{mod}}} - I_{R_{obs}})^T R_I^{-1} (I_{R_{\mathrm{mod}}} - I_{R_{obs}}) + (P_{\mathrm{mod}} - P_{obs})^T R_P^{-1} (P_{\mathrm{mod}} - P_{obs}), \quad (5)$$

where I_{Rmod} and I_{Robs} are vectors of the modeled and observed regional inventories, P_{mod}, and P_{obs} are vectors of the initial and optimized control parameters and R_I, and R_P are the covariance matrices for the inventories and control parameters, respectively. In minimizing equation (5), it was assumed that the individual inventory observations and the

Table 4. Results of the Inverse Calculation Showing the Optimized Value for Each of the Terms in the Model and the Reduction in the Cost Function, J, by the Optimization[a]

Parameter	x_0	Optimal Value	Range (16 Runs)
C_V/C_P	0.7 ± 0.1	0.67	0.60–0.74
Indonesian Throughflow	10 ± 10 Sv	15.8 Sv	10.6–19.1 Sv
Subduction rate	30 ± 5 Sv	26.4 Sv	20.9–28.8 Sv
Subduction timescale	10 ± 2 years	9 years	8–10 years
NPIW	5 ± 5 Sv	5.5 Sv	4.9–6.3 Sv
Arctic outflow	1 ± 0.2 Sv	1.0 Sv	1.00–1.01 Sv
NPIW outflow	5 ± 2 Sv	5.7 Sv	4.5–7.0 Sv
J	8.18	3.17	1.10–10.64

[a]The range of optimal values shown in the third column is the result of the second Monte Carlo analysis where I_{Robs} was randomly perturbed to see how well the model and data can constrain the deposition and circulation terms.

control parameters are all uncorrelated, and thus R_I and R_P are simple diagonal matrices. The diagonal terms in the covariance matrices are the variances in each of the inventories and control parameters. As the overall error in the WOCE North Pacific inventory is approximately 10% (Table 1), a 10% uncertainty in each of the regional inventory values was assumed in equation (5). Mass was conserved at all times as model mass balance was calculated at each iteration during the inversion. Equation (5) was minimized using a multidimensional unconstrained nonlinear minimization approach (MATLAB™ fminsearch), which is a Nelder-Mead type scheme. The first guess at each of the parameter values (x_0) was that used in the original model run and is given, along with its associated uncertainty, in Table 4. An additional constraint was also placed on the C_V/C_P ratio to prevent it from exceeding the isotopic equilibrium value of 0.89.

6.1. Stability of the Solution

[54] The cost function surface was explored in three ways to assess the stability of the solution. First, the values of x_0, the initial guess of the parameter values, were varied from $0.1x_o$ to $10x_0$, which did not change the value of J or the optimal values of the control parameters. Second, a simple Monte Carlo analysis was done where the starting point was perturbed using a set of Gaussian distributed random values. The values, generated using the MATLAB™ ''randn'' function, had a mean of zero and a standard deviation that was set as equal to the uncertainty in each term (Table 4). All optimizations with these randomly generated perturbations yielded the same values for both the control parameters and the cost function, J. The robustness of the minimization under these two tests led to the conclusion that the solution is stable and indicates that the minimization scheme has not found a local minimum.

[55] Finally, a second Monte Carlo analysis was performed to assess the robustness of the optimal parameters and determine how well the combination of the multibox model and WOCE data is constraining them. To do this, the WOCE regional inventories, I_{Robs}, were randomly perturbed, again using a set of Gaussian distributed random values, this time with a mean of zero and standard deviation set to 10% of the inventory values, the uncertainty in the WOCE regional ^{3}H inventories. The results of 16 such randomly generated analyses are shown in Table 4 and show that the values of the control parameters vary by up to 30% depending on the inventories used, with only the magnitude of the Arctic outflow being unaffected. This implies that to further constrain atmospheric deposition and North Pacific circulation using ^{3}H data, either the ^{3}H inventory and distribution within this ocean needs to be better constrained or more of the spatial information in the tritium data needs to be exploited using a more realistic circulation model, or both in combination. The tight constraint on the Arctic outflow may indicate that small changes in its value have a significant impact on the inventory in the subpolar surface box, which, as is discussed below, is not recreated well by the model.

6.2. Results of the Inverse Solution

[56] The inventory values presented in Table 3 indicate that the minimization has improved the agreement between the model and the WOCE data, as is borne out by the reduction in the value of the cost function (Table 4). The overall inventory for the basin produced by the optimization is in very close agreement with the calculated WOCE value (23.12 kg compared with the WOCE value of 23.40 kg), and regionally the ^{3}H distribution is also improved. The tropical and total subpolar inventories are now within 10% of the WOCE values, which was not true of the original model run. However, looking at the depth distribution in the subpolar boxes indicates that although the optimization improves the agreement with the data, the inventory in the deep box is still overestimated. This indicates that the model may not be capable of accurately recreating the WOCE ^{3}H distribution north of 40°N and that some aspect of the circulation in the basin is not being represented. It may be the lack of intermediate depth circulation at subtropical and tropical latitudes that is causing the model to have difficulty replicating the ^{3}H distribution, as it is assumed that water only flows from intermediate subpolar depths to the subtropical surface box.

[57] The optimal values of the model parameters are presented in Table 4, which shows that they all fall within the range of literature estimates, highlighting tritium's ability to constrain circulation. It is clear that the overall inventory requires a C_V/C_P ratio of around 0.67 (range 0.60–0.74), which is less than isotopic equilibrium but certainly not as small as was indicated by the *Koster et al.* [1989] modeling work. Similar results were found for the North Atlantic [*Doney et al.*, 1993]. The observed ^{3}H inventories for these two basins are simply too large to be supported mainly by direct precipitation input and thus require a substantial vapor transport pathway as river input and ocean lateral transport are insufficient to make up the difference. This discrepancy emphasizes the need for a more thorough examination of the isotopic transport pathways for liquid and vapor forms of water in the atmosphere.

[58] The inverse model simulations tend to indicate an Indonesian Throughflow on the higher end of observation based estimates, which is likely driven by the model in an attempt to lower the excess ^{3}H inventory in the tropics. It is somewhat striking that the ^{3}H based estimate of the throughflow by *Fine* [1985] is, in contrast, at the lower end of the observational range (~5 Sv). If that number is believable, then either the ^{3}H deposition is poorly represented in the tropics or another mechanism, such as the subtropical cell, is required to decrease the tropical budget.

7. Summary

[59] In this study, tritium data from the WOCE series of cruises were used to construct improved basin-scale and regional ^{3}H inventories for the North Pacific. These were then used as constraints to develop a budgetary model of the basin to explain the evolving ^{3}H distribution for this ocean. To achieve this, an improved precipitation function was constructed, and both this and the budgetary model performed well when compared with the available observations. In calculating the precipitation function, a third factor emerged that was not seen in the *Doney et al.* [1992] analysis, the temporal evolution of which highlighted the importance of direct ^{3}H deposition at the time of the thermonuclear weapons tests. As with earlier calculations

[*Doney et al.*, 1993], the uncertainty associated with the atmospheric deposition of ^{3}H to the oceans is the greatest weakness of the model. The relationship between the ^{3}H concentration in water vapor and precipitation remains problematic, as does the air-sea vapor flux and the length scale of the continent-marine transition.

[60] The unadjusted ^{3}H budget model overestimates the basin inventory based on the WOCE data by ~7%, but this error is well within the uncertainty of the atmospheric deposition. The solution of an inverse calculation highlights that despite the uncertainty in the atmospheric deposition terms, it is possible to put constraints on circulation using ^{3}H data. However, for tighter constraints to be placed on circulation terms, it may be necessary to take advantage of the spatial knowledge of ^{3}H in the North Pacific by utilizing a more sophisticated circulation model for the basin.

[61] The lack of oceanic tritium in precipitation data, the limited data available on the C_V/C_P ratio and the continent-marine transition length scale are likely to be the main sources of model error. It is clear that these factors limit the usefulness of ^{3}H in constraining and testing circulation and ocean models at present, as is highlighted by the model's difficulty in reproducing the depth partitioning of ^{3}H at high latitudes. Without more knowledge about these terms, high-resolution model ^{3}H simulations should be treated with care, though a GCM run could provide a far more detailed spatial structure and transport of ^{3}H within the North Pacific, or any other basin, than was possible in this work. To optimize the use of ^{3}H in such roles, for which the isotope could be very useful due to the large number of measurements made as part of the WOCE program, it is essential to improve the surface boundary condition and in particular the C_V/C_P ratio. To improve the knowledge of the C_V/C_P ratio there either needs to be a detailed field study of ^{3}H concentrations in maritime air masses or a high resolution atmospheric model of vapor transport in the atmosphere needs to be run.

[62] However, it is possible that the lack of oceanic ^{3}H in precipitation data may be improved in the future. Tritium bound in the cellulose of tree rings at oceanic islands has the potential to provide a record of past precipitation that could be used to improve the isotope's surface boundary condition. Such reconstructions have been done for deuterium (^{2}H) and a strong correlation has been found between the cellulose deuterium concentrations and those of their associated waters [*Epstein et al.*, 1976; *Schiegl*, 1974]. In such reconstructions the precipitation signal can be complicated by contributions from groundwater, vapor and fractionation during biosynthesis. However, a careful choice of tree and study of the fractionation steps involved should allow accurate precipitation ^{3}H reconstructions to be made. With the information that this technique has the potential to provide, ^{3}H could become a very powerful tool to study circulation and constrain general circulation models.

[63] **Acknowledgments.** Support for this work was provided by UK Natural Environment Research Council grant GR3/12800, and by the U.S. National Science Foundation grant OCE26080500. Support for sample acquisition and laboratory analysis was provided by numerous NSF grants under the WOCE program, and we are grateful to the many chief scientists and dedicated seagoing technicians for their hard work. Thanks also to Dempsey Lott III for making the tritium program work.

References

Baumgartner, A., and E. Reichel (1975), *The World Water Balance*, 179 pp., Elsevier, New York.

Broecker, W. S., T. H. Peng, and G. Östlund (1986), The distribution of bomb tritium in the ocean, *J. Geophys. Res.*, *91*, 14,331–14,344.

Da Silva, A., A. C. Young, and S. Levitus (1994), *Atlas of Surface Marine Data 1994*, vol. 1, *Algorithms and Procedures*, *NOAA Atlas NESDIS 6*, Natl. Oceanic and Atmos. Admin., Silver Spring, Md.

Doney, S. C., D. M. Glover, and W. J. Jenkins (1992), A global model function of the tritium concentration in precipitation, 1960–1986, *J. Geophys. Res.*, *97*, 5481–5492.

Doney, S. C., W. J. Jenkins, and H. G. Östlund (1993), A tritium budget for the North Atlantic, *J. Geophys. Res.*, *98*, 18,069–18,081.

England, M. H., and E. Maier-Reimer (2001), Using chemical tracers to assess ocean models, *Rev. Geophys.*, *39*, 29–70.

Epstein, S., C. J. Yapp, and J. H. Hall (1976), The determination of the D/H ratio of non-exchangeable hydrogen in cellulose extracted from aquatic and land plants, *Earth Planet. Sci. Lett.*, *30*, 214–251.

Fieux, M., R. Molcard, and A. G. Ilahude (1996), Geostrophic transport of the Pacific-Indian Oceans throughflow, *J. Geophys. Res.*, *101*, 12,421–12,432.

Fine, R. A. (1985), Direct evidence using tritium data for throughflow from the Pacific into the Indian Ocean, *Nature*, *315*, 478–480.

Fine, R. A., and H. G. Östlund (1977), Source function for tritium transport models in the Pacific, *Geophys. Res. Lett.*, *4*, 461–464.

Fine, R. A., J. L. Reid, and H. G. Östlund (1981), Circulation of tritium in the Pacific Ocean, *J. Phys. Oceanogr.*, *11*, 3–14.

Fine, R. A., W. H. Peterson, and H. G. Östlund (1987), The penetration of tritium into the tropical Pacific, *J. Phys. Oceanogr.*, *17*, 553–564.

Godfrey, J. S. (1996), The effect of the Indonesian throughflow on ocean circulation and heat exchange with the atmosphere: A review, *J. Geophys. Res.*, *101*, 12,217–12,237.

Gordon, A. L. (1986), Inter-ocean exchange of thermocline water, *J. Geophys. Res.*, *91*, 5037–5046.

Huang, R. X., and S. Russell (1994), Ventilation of the subtropical North Pacific, *J. Phys. Oceanogr.*, *24*, 2589–2605.

Itoh, M., K. I. Ohshima, and M. Wakatsuchi (2003), Distribution and formation of Okhotsk Sea Intermediate Water: An analysis of isopycnal climatological data, *J. Geophys. Res.*, *108*(C8), 3258, doi:10.1029/2002JC001590.

Jean-Baptiste, P., and M. J. Messias (1993), Using tracers to study ocean circulation: What more can we learn by the year 2000?, *Ann. Inst. Oceanogr.*, *69*, 283–305.

Johnson, G. C. (2001), The Pacific Ocean subtropical cell surface limb, *Geophys. Res. Lett.*, *28*, 1771–1774.

Jouzel, J., J. G. Russell, R. Suozzo, R. Koster, J. W. C. White, and W. S. Broecker (1987), Simulations of the HDO and $H_2^{18}O$ atmospheric cycle using the NASSA/GISS General Circulation Model: The seasonal cycle for present-day conditions, *J. Geophys. Res.*, *92*, 14,739–14,760.

Key, R. M. (2001), Ocean process tracers: Radiocarbon, in *Encyclopedia of Ocean Sciences*, edited by J. Steele, S. Thorpe, and K. Turekian, pp. 2338–2353, Academic, San Diego, Calif.

Koster, R. D., W. S. Broecker, J. Jouzel, R. J. Suozzo, G. L. Russell, D. Rind, and J. W. C. White (1989), The global geochemistry of bomb-produced tritium: General circulation model compared to available observations and traditional interpretations, *J. Geophys. Res.*, *94*, 18,305–18,326.

Li, X., and C. Wunsch (2003), Constraining the North Atlantic circulation between 4.5°S and 39.5°N with transient tracer observations, *J. Geophys. Res.*, *108*(C10), 3318, doi:10.1029/2002JC001765.

Liu, Z., and B. Huang (1998), Why is there a tritium maximum in the central equatorial Pacific thermocline?, *J. Phys. Oceanogr.*, *28*, 1527–1533.

Liu, Z., and G. Philander (2001), Tropical-extratropical oceanic exchange pathways, in *Ocean Circulation and Climate: Observing and Modeling the Global Ocean*, edited by G. Siedler, J. Church, and W. J. Gould, pp. 247–254, Academic, San Diego, Calif.

Lucas, L. L., and M. P. Unterweger (2000), Comprehensive review and critical evaluation of the half-life of tritium, *J. Res. Natl. Inst. Standard Technol.*, *105*, 541–549.

Mahadevan, A. (2001), An analysis of bomb radiocarbon trends in the Pacific, *Mar. Chem.*, *73*, 273–290.

McCreary, J. P., and P. Lu (2001), Influence of the Indonesian throughflow on the circulation of Pacific Intermediate Water, *J. Phys. Oceanogr.*, *31*, 932–942.

McPhaden, M. J., and R. A. Fine (1988), A dynamical interpretation of the tritium maximum in the central equatorial Pacific, *J. Phys. Oceanogr.*, *18*, 1454–1457.

Memery, L., and C. Wunsch (1990), Constraining the North Atlantic Circulation with tritium data, *J. Geophys. Res.*, *95*, 5239–5256.

Michel, R. L., and H. E. Suess (1975), Bomb tritium in the Pacific Ocean, *J. Geophys. Res.*, *80*, 4139–4152.
Morey, S. L., J. F. Shriver, and J. J. O'Brien (1999), The effects of Halmahera on the Indonesian throughflow, *J. Geophys. Res.*, *104*, 23,281–23,296.
Östlund, H. G. (1982), The residence time of the freshwater component in the Arctic Ocean, *J. Geophys. Res.*, *87*, 2035–2043.
Östlund, H. G., and A. S. Mason (1985), Atmospheric tritium, 1968–1984, in *Tritium Laboratory Data Report*, 134 pp., Rosenstiel School of Mar. and Atmos. Sci., Univ. of Miami, Miami, Fla.
Peixoto, J. P., and A. H. Oort (1983), The atmospheric branch of the hydrological cycle and climate, in *Variations in the Global Water Budget*, edited by A. Street-Perrott, M. Beran, and R. Ratcliffe, pp. 5–65, D. Reidel, Norwell, Mass.
Peng, T. H., R. M. Key, and H. G. Östlund (1998), Temporal variations of bomb radiocarbon inventory in the Pacific Ocean, *Mar. Chem.*, *60*, 3–13.
Potemra, J. T., R. Lukas, and G. T. Mitchum (1997), Large-scale estimation of transport from the Pacific to the Indian Ocean, *J. Geophys. Res.*, *102*, 27,795–27,812.
Prabhakara, C., H. D. Chang, and A. T. C. Chang (1982), Remote sensing of precipitable water over the oceans from Nimbus 7 microwave measurements, *J. Appl. Meteorol.*, *21*, 59–68.
Qiu, B., and R. X. Huang (1995), Ventilation of the North Atlantic and North Pacific: Subduction versus obduction, *J. Phys. Oceanogr.*, *25*, 2374–2390.
Reid, J. L. (1965), Intermediate waters of the Pacific Ocean, *Johns Hopkins Oceanogr. Stud.*, *2*, 85 pp.
Rodgers, K. B., M. A. Cane, N. H. Naik, and D. P. Schrag (1999), The role of the Indonesian Throughflow in equatorial Pacific thermocline ventilation, *J. Geophys. Res.*, *104*, 20,551–20,570.
Roether, W. (1989), An account of tritium in the ocean, special report, 21 pp., Int. Atomic Energy Agency, Vienna.
Schiegl, W. E. (1974), Climatic significance of deuterium abundance in growth rings of *Picea*, *Nature*, *251*, 582–584.
Talley, L. D. (1991), An Okhotsk Sea water anomaly: Implications for ventilation in the North Pacific, *Deep Sea Res.*, *38*(1), 171–190.
Talley, L. D. (1993), Distribution and formation of North Pacific Intermediate Water, *J. Phys. Oceanogr.*, *23*, 517–537.
Talley, L. D., and J. Y. Yun (2001), The role of cabelling and double diffusion in setting the density of the North Pacific Intermediate Water salinity minimum, *J. Phys. Oceanogr.*, *31*, 1538–1549.
Taylor, C. B. (1966), Tritium in Southern Hemisphere precipitation 1953–1964, *Tellus*, *18*, 105–131.
Taylor, C. B. (1971), Influence of 1968 French thermonuclear tests on tritium fallout in the Southern Hemisphere, *Earth Planet Sci. Lett.*, *10*, 196–198.
Van Scoy, K. A., R. A. Fine, and H. G. Östlund (1991), Two decades of mixing tritium into the North Pacific Ocean, *Deep Sea Res.*, *38*, Suppl. 1, S191–S219.
Warner, M. J., and G. I. Roden (1995), Chlorofluorocarbon evidence for recent ventilation of the deep Bering Sea, *Nature*, *373*, 409–412.
Warner, M. J., J. L. Bullister, D. P. Wisegarver, R. H. Gammon, and R. F. Weiss (1996), Basin-wide distributions of chlorofluorocarbons CFC-11 and CFC-12 in the North Pacific: 1985–1989, *J. Geophys. Res.*, *101*, 20,525–20,542.
Weiss, W., and W. Roether (1975), Der Tritiumabfluss des Rheins 1961–1973, *Dtsch. Gewässerkd. Mitt.*, *19*, 1–5.
Weiss, W., and W. Roether (1980), The rates of tritium input to the world oceans, *Earth Planet. Sci. Lett.*, *49*, 435–446.
Weiss, W., W. Roether, and E. Dreisigacker (1979), Tritium in the North Atlantic: Inventory, input and transfer into the deep water, in *The Behaviour of Tritium in the Environment*, pp. 315–336, Int. Atomic Energy Agency, Vienna.
Wong, C. S., R. J. Matear, H. J. Freeland, F. A. Whitney, and A. S. Bychkov (1998), WOCE line P1W in the Sea of Okhotsk: 2. CFCs and the formation rate of intermediate water, *J. Geophys. Res.*, *103*, 15,625–15,642.
Yasuda, I., K. Okuda, and Y. Shimizu (1996), Distribution and modification of North Pacific Intermediate Water in the Kuroshio-Oyashio interfrontal zone, *J. Phys. Oceanogr.*, *26*, 448–465.

S. C. Doney and W. J. Jenkins, Woods Hole Oceanographic Institution, Woods Hole, MA 02543, USA. (sdoney@whoi.edu; wjenkins@whoi.edu)
S. Stark, Hadley Centre for Climate Prediction and Research, Fitzroy Road, Exeter EX APB, UK. (sheila.stark@metoffice.com)